Three-dimensional fruit growth analysis clarifies developmental mechanisms underlying complex shape diversity in persimmon fruit

Akane Kusumi, Soichiro Nishiyama, Ryutaro Tao

Graduate School of Agriculture, Kyoto University, Sakyo-ku, Kyoto 606-8502, Japan

Correspondence: Soichiro Nishiyama (e-mail: nishiyama.soichiro.8e@kyoto-u.ac.jp, TEL: +81-75-753-6051)

Abstract

How fruit size and shape are determined is of research interest in agriculture and developmental biology. Fruit typically exhibits three-dimensional structures with genotype-dependent geometric features. Although minor developmental variations have been recognized, little research has fully visualized and measured these variations throughout fruit growth. In this study, a high-resolution 3D scanner was used to investigate the fruit development of 51 persimmon (*Diospyros kaki*) cultivars with various complex shapes. We obtained 2,380 3D fruit models that fully represented fruit appearance, and enabled precise and automated measurements of unique geometric features throughout fruit development. The 3D fruit model analysis identified key stages that determined the shape attributes at maturity. Typically, genetic diversity in vertical groove development was found, and such grooves can be filled by tissue expansion in the carpal fusion zone during fruit development. Furthermore, transcriptome analysis of fruit tissues from groove/non-groove tissues revealed gene co-expression networks that were highly associated with groove depth variation. The presence of *YABBY* homologs was most closely associated with groove depth and indicated the possibility that this pathway is a key molecular contributor to vertical groove depth variation. These results demonstrate the validity of fruit 3D growth analysis, which is a powerful tool for identifying the developmental mechanisms of fruit shape variation and the molecular basis of this diversity.

Keywords: *Diospyros kaki*; fruit shape; phenotyping; 3D measurement; *YABBY*

Introduction

Fruit is an organ of angiosperms that facilitates reproduction. Generally, the fruit ovary protects seeds until they mature and promotes seed dispersal once fruit has reached maturity by color or aroma to attract animals (Howe and Smallwood, 1982). Fruits are classified by three characteristics: dehiscence or indehiscence, dry or fleshy, and unfused or fused carpels (Seymour et al. 2013). Fruit with fused carpels evolved from organs that are homologous to leaves (Scutt et al., 2006). Many studies demonstrated that mutations of genes related to floral development resulted in conversion of flowers into leaves, and that ectopic expression of those genes could transform leaves into floral organs and vice versa (Ferrándiz et al., 2010; Honma and Goto, 2001). After floral organ development is completed, fertilization stimulates hormonal and genetic change in ovules and ovaries; thus, fruit development is triggered (Mezzetti et al., 2004; Eklund et al., 2010). Fleshy fruit development is typically driven by cell division at the early stage and subsequently there is cell expansion (Gillaspy et al., 1993). Several major genes have been identified as affecting the final fruit size or shape by regulating the speed and direction of cell division and expansion (van der Knaap et al., 2014).

Fruit shape is an important agricultural trait and has been targeted in breeding (Cliff et al., 2002). In agricultural research practices, fruit shape has been evaluated by descriptive rating scales or 2D imaging of fruit. In particular, 2D imaging has been used for many species with various fruit shapes, such as tomato, cucumber, apple, and litchi (Gonzalo et al., 2009; Shimomura et al., 2016; Currie et al., 2000; Osako et al., 2020). In most cases, 2D imaging methods acquire images from one side of the fruit or from a sliced cross section, and shape features are obtained by image processing. Although 2D imaging-based quantitative evaluation of fruit shape is advantageous because the data collection can be quick, inexpensive, and simple, there are also disadvantages. Ding et al. (2000) found that the biggest disadvantage of 2D fruit morphology evaluation is that there is missing or reduced information. Two-dimensional evaluation often fails to capture part of the shape features that the original 3D structure possesses in that it represents only a single side of fruit and thus important information can be obscured. For this reason, 3D plant phenotyping has emerged and been applied in some important crops such as potato and strawberry (Liu et al., 2021; He et al., 2017; Li et al., 2020). Recent advances in photogrammetry have facilitated 3D image acquisition, yet very few studies have employed this technology to assess genetic diversity in fruit development.

Cultivated oriental persimmon (*Diospyros kaki* Thunb.), a temperate deciduous fruit tree, shows unique genetic variations in fruit development and shape (Nishiyama and Yamane, 2022). Regarding overall shape, some are flat, such as 'Hiratanenashi,' but others are elongated, such as 'Fudegaki.' In addition, some cultivars develop vertical and horizontal grooves ("Mizo" and "Za" in Japanese) in the lateral side and the proximal (calyx) end of the fruit, respectively, adding unique diversity to persimmon fruit shape (Fig. 1a and 1b). Conventionally, persimmon fruit shape diversity has been categorized into phenotype classes (Fruit Tree Experiment Station of Hiroshima Prefecture, 1979; UPOV, 2004). For example, vertical groove depth was evaluated using a score and descriptor, such as "7. deep," "3. shallow, but obvious," or "1. absent" in the report by Fruit Tree Experiment Station of Hiroshima Prefecture (1979). Similarly, horizontal grooves were evaluated as "9. extremely big," "3. small," or "1. absent." However, this qualitative categorization can produce confusion. In Fig. 1a, 'Mizushimagosho' and 'Amayotsumizo' were classified as having vertical grooves at the same level, though the actual depths are quite different. Therefore, developing a quantitative measurement method for persimmon fruit is beneficial in both agriculture and fruit development research.

Maeda et al. (2018) phenotyped persimmon fruit by chronologically applying an elliptic Fourier descriptors-based PCA method for 2D images of 153 *D. kaki* cultivars and two related species. The 2D imaging method successfully represented the ratio of length to diameter and the fruit shape of the distal (apex) end, whereas components representing vertical and horizontal grooves were not detected. In fact, when the entire fruit is photographed from one direction, as in Maeda et al. (2018), the grooves in persimmon fruit are often self-occluded (Fig. 1c); thus, measurement by 2D-based methods is difficult. Ding et al. (2000) developed a 3D morphological analysis method for persimmon fruit. They captured the whole fruit contours using a CCD laser sensor system; however, there were few data points, and development of the unique persimmon fruit characteristics, such as horizontal and vertical grooves, have not yet been fully evaluated.

We previously showed potential applicability of photogrammetry-based 3D phenotyping of groove depths in persimmon fruit; shape measurements by geometric processing of the obtained 3D models represented the genetic diversity in the pattern of vertical groove depth (Kusumi et al., 2022). In this study, we applied a high-resolution 3D scanner to model the full growth of persimmon fruits with diverse shapes and to obtain regulatory information regarding fruit morphological development. In addition, transcriptome analysis was conducted to characterize the

molecular mechanism of vertical groove regulation.

Materials and Methods

Plant materials

Fruit shapes were assessed for 51 *D. kaki* cultivars planted in the Kyoto Farmstead of the Experimental Farm of Kyoto University (Kyoto, Japan) (Table 1). Four to six fruits were sampled from each cultivar every 2 weeks, starting from the flowering stage in mid-May until the end of growth stage 1 in mid-August, and every 4 weeks after that until maturity, which varied among cultivars from the end of September to the beginning of November. The sampling interval was adjusted because it is known that the persimmon fruit growth follows a double-sigmoid curve, with growth stage 1 corresponding to the period when fruit development is drastically driven by active cell division and cell expansion (Nii, 1980), and its shape does not change rapidly after approximately 10 weeks after blooming (WAB). However, due to the rottenness during the storage, 'Mizushimagosho' of 16 WAB contained only 2 fruits.

Acquiring 3D models

A 3D Scanner Coordinate Measuring Machine (VL-500; KEYENCE, Osaka, Japan) was used to develop 3D models of the persimmon fruit. Fruit was sampled with the peduncle at the first 2 sampling periods, which were 0 and 2 WAB, and the fruit was scanned with the peduncle. After 4 WAB, the fruit calyx was removed to scan the precise features around it. Each persimmon fruit was set on a rotating table, and 3D images were obtained every 30 or 60 degrees; the interval at which images were taken (30 or 60 degrees) was based on sample complexity. The turning angle was optimized according to the fruit shape complexity, and image acquisition was iterated until a high-quality 3D model was obtained. This step was done for both side of each fruit, i.e., the proximal end and distal end, which led to an intact fruit 3D model when they were fused (Fig. 1c). The final model was saved as an STL file. All 3D models developed in this study are available at https://doi.org/10.6084/m9.figshare.22001908.

Image processing

MeshLab version 2021.05 (Cignoni et al., 2008), trimesh version 3.17.1 (https://github.com/mikedh/trimesh), and OpenCV version 3.1.0 (Bradski, 2000) were used to process 3D models and measure shape features, and the code is available at https://github.com/pomology-ku/persimmon-fruit-3D-measurement. Regarding the samples from 0 and 2 WAB, peduncles were manually removed using MeshLab. For all fruit models, the Z-axis was aligned to the proximal-distal line. Horizontal sections in the XY-plane were obtained by dividing the fruit model into 100 equal parts along the Z-axis. Additionally, 30 vertical sections were acquired by slicing the model by every 6° from the centroid origin.

Based on horizontal sections, vertical groove and roundness parameters were measured (Fig. 2a and Supplementary Fig. 1a). A parameter that represented vertical groove depth, Groove Index (GI), and Roundness (Ro) were calculated by the following equations:

$$Groove\ Index\ (GI) = \frac{Area\ of\ convexity\ defect}{Area\ of\ horizontal\ section}$$

$$Roundness\ (Ro) = \frac{Diameter\ of\ maximum\ inscribed\ circle\ of\ contour}{Diameter\ of\ minimum\ circumscribed\ circle\ of\ contour}$$

Length to width (L/W) ratio and horizontal grooves were evaluated from transverse sections. L/W ratio was calculated by the average of L/W from 30 sections (Fig. 3a). After detecting horizontal grooves based on curvature change, groove location was identified as the angle between the proximal–distal line and the line connecting the origin and detected groove. Groove location was averaged across 30 sections for each sample. It should be noted that horizontal groove measurement was conducted for eight cultivars with visible horizontal grooves (Table 1).

Finally, Tukey–Kramer's multiple comparison test ($p < 0.05$) was performed among different developmental stages to determine when these morphological parameters were fixed. The stage when the shape parameter score had no significant difference from mature fruit was considered the stage at which shape attributes were determined.

132 *Microscopic observation*

133 Five fruits from each of four cultivars (‘Mizuhimagosho,’ ‘Saijou,’ ‘Amayotsumizo,’ and ‘Fuyuu’), which
134 exhibited various GI at blooming, were sampled at anthesis in mid-May 2022. They were then fixed in the fixative
135 FAA (formalin: acetic acid: ethanol: distilled water = 2:1:10:7 v/v/v/v), followed by dehydration in a graded ethanol
136 series. Samples were cryo-embedded in blocks and cut into 6- or 8-µm-thick sections according to Kawamoto (1990).
137 Sections stained with toluidine blue were observed with an optical microscope (BX53FL, OLYMPUS, Tokyo, Japan).

138 Cell numbers and sizes were calculated as follows: first, baselines connecting the tips of seeds inside a fruit
139 were drawn (Fig. 4d). Second, line G (grooved zone) or N (non-grooved zone) was set from baseline to the point at
140 the contour of the fruit where the groove was deepest, or the point where the distance to the baseline was the longest.
141 Finally, number and size of cells that overlap with line G or N were measured. Parenchyma and tannin cells were
142 independently measured (Fig. 4e). To reduce the effect of outliers on cell size, the upper and lower 5% of data were
143 removed, and mean was calculated with the other 90% of the data. Wilcoxon rank sum test was conducted to assess
144 if there was significant difference between groove-present and -absent zones.

145

146 *Transcriptome analysis*

147 Fruits were sampled from eight cultivars (‘Zenjimaru,’ ‘Fuyuu,’ ‘Amayotsumizo,’ ‘Fujiwaragosho,’
148 ‘Gionbou,’ ‘Saijou,’ ‘Iwasedo,’ and ‘Mizushimagosho’) at 4 WAB (10 June 2022). Those cultivars were selected
149 because the vertical groove depth plateaus at around or after 4 WAB (except ‘Zenjimaru,’ which reached plateaus at
150 around 2 WAB). The grooved and non-grooved zones for each sample (Fig. 5a) were cut from each fruit, and the peel
151 and developing seeds were removed. Each tissue from each fruit was considered a single biological replicate, and
152 four or five fruits (replicates) were prepared for each cultivar and tissue type.

153 Total RNA was extracted by the hot borate method (Wan and Wilkins, 1994). Extracted RNA was quantified
154 using a Qubit 4 fluorometer (Invitrogen, Carlsbad, CA, USA). In total, 500 ng of total RNA was used to prepare
155 mRNAseq libraries. mRNAseq libraries were prepared using the NEBNext® Poly(A) mRNA Magnetic Isolation
156 Module, NEBNext® Ultra™ II RNA Library Prep Kit for Illumina®, and NEBNext® Multiplex Oligos for Illumina®
157 (New England Biolabs, Ipswich, MA, USA) following the manufacturer’s recommendations. The 78 libraries were

158 split into two groups of 40 and 38 to avoid barcode sequence overlap, and they were sequenced in one lane of
159 DNBSEQ (PE150) for each pool at Azenta Inc, Japan (Tokyo, Japan). All RNA samples used for RNAseq analysis
160 are listed in Supplementary Table 1. All sequence data are available in the DDBJ Sequenced Read Archive (accession
161 number DRA015493).

162 All sequences were pre-processed using fastp (Chen et al., 2018) with a minimum read length threshold of
163 35 bp. The reads from each library were aligned to the *Diospyros oleifera* reference genome (Suo et al., 2020) using
164 STAR with default parameters (Dobin, et al., 2013). Alignments were sorted using SAMtools (Li et al., 2009), and
165 the number of reads mapped to each contig was counted from the BAM files using HTseq-count (Putri et al., 2022).
166 Gene expression level was represented as transcripts per million (TPM).

167 Differential expression between grooved and non-grooved zones in groove-present cultivars was evaluated
168 using Deseq2 version 1.34.0 (Love et al., 2014) with the cultivar factor being input as cofactor of the model. A false
169 discovery rate of 0.05 was set to define differentially expressed genes (DEGs). Genes in the *D. oleifera* reference
170 genome was functionally annotated using eggNOG 5.0 (Huerta-Cepas et al., 2019) with default parameters. Gene
171 ontology enrichment analysis of the groove-associated DEGs was conducted using goseq (Young et al., 2010) with a
172 false discovery rate of 0.1 as the significance threshold. A gene co-expression network was constructed using
173 WGCNA (Langfelder and Horvath, 2008) with a TPM matrix for genes with TPM > 1 and the following parameters:
174 minModuleSize = 30, mergeCutHeight = 0.25. Soft thresholding power was set to 9, with a scale-free topology fitting
175 index of $R^2 > 0.85$. The gene module containing the *YABBY* homologs and network edges with topological overlap
176 greater than 0.30 was visualized using R package visNetwork version 2.1.2 (https://github.com/datastorm-
177 open/visNetworkg).

178

179

180 **Results**

181 *Three-dimensional modeling of persimmon fruit*

182 The VL-500 3D scanner developed fruit 3D models that precisely reflected morphological features of
183 persimmon fruit, including horizontal and vertical grooves (Fig. 1c, d). The polygon meshes of fruit 3D models

184 included at least 120 vertices per mm^2, which is sufficiently fine to evaluate fruit shape at flowering (*ca.* 4.08 mm in
185 longitudinal diameter) in the cultivar with the smallest ovary at flowering, 'Totsutanenashi.' Examples of horizontal
186 sections from 'Ooniwa' and 'Saijou' are shown in Fig. 1d. The slice contours showed clear grooves, and the models
187 included genetic differences in groove depth, including in 'Ooniwa,' which has deeper grooves and a deeper cavity
188 at the grooved zone. These general features of 3D models supported the feasibility of evaluating complex shape
189 attributes based on cross sections of the 3D models.
190
191 *Characterization of vertical groove disappearance using 3D modeling*
192 To acquire a reliable metric to measure the shape attributes, GI and Ro were visualized over cross sections
193 from the proximal to the distal end (Fig. 2a and Supplementary Fig. 1a). The contours in horizontal sections near the
194 proximal or distal ends were often rough and not stable because of concavity at both ends (Fig. 2b and Supplementary
195 Fig. 1b). Thus, GI and Ro were only evaluated from section #20-89, and were named GI#20-89 and Ro#20-89,
196 respectively.
197 Fig. 2c represents the chronological change in GI#20-89 from all cultivars as clustered by Euclidean
198 distance. The cultivars with vertical grooves clustered in conventional categories but were largely separated into two
199 groups according to change pattern. We observed that all analyzed cultivars had vertical grooves in fruit at flowering,
200 and GI#20-89 decreased as fruit developed. By 6 WAB at the latest, the groove shape of 47/51 analyzed cultivars
201 showed GI#20-89 values consistent with the value at maturity, with the remaining four cultivars determined at 8
202 WAB (Table 1). Therefore, vertical groove depth was mainly determined in the initial stage of fruit development, at
203 which time active cell division rather than cell expansion takes place.
204
205 *Roundness and its association with vertical groove depth*
206 Roundness was also evaluated from transverse sections. Supplementary Fig. 1 shows a chronological
207 change in Ro#20-89 for all cultivars, as classified by Euclidean distance. Generally, Ro#20-89 tended to increase
208 with development, which indicated that the fruit became round during development. Interestingly, cultivars with
209 vertical grooves generally clustered together; these cultivars tended to be less round. In most cultivars, roundness

210 reached at the maturity level by 10 WAB (Table 1).

211 To further investigate the relationship between the groove depth and roundness, Spearman's rank
212 correlation analysis was performed. Through developmental stages, groove depth and roundness were significantly
213 correlated with each other ($p < 0.01$) (Supplementary Fig. 2a), which indicated that grooved fruit tends to be square-
214 shaped. At 0 WAB, the correlation coefficient was −0.518. Then, the coefficient gradually increased and reached
215 −0.743 at maturity (Supplementary Fig. 2b). This result implies a common mechanism underlying both vertical
216 groove depth and roundness.

217

218 *Horizontal groove and L/W development during fruit growth*

219 Horizontal grooves and L/W development were evaluated using 30 vertical sections of each fruit (Fig. 3a).
220 Supplementary Fig. 3a shows a chronological change in L/W for all cultivars, as classified by Euclidean distance.
221 L/W remained low through the development of flat cultivars; however, it increased toward maturity in oblong
222 cultivars. 'Fudegaki' and 'Nagara,' which have oblong fruit, exhibited drastic changes in L/W. L/W was determined
223 within the first developmental stage in most cultivars, but there were several cultivars whose L/W was not determined
224 by 24 WAB. Cultivars with late determination included many oblong cultivars, such as 'Nagara,' 'Fudegaki,' 'Saijou,'
225 and 'Aburatsubo.'

226 Detecting horizontal grooves was difficult and produced many missing values. This is because the grooves
227 typically did not cover the entire fruit, or the curvature change at the grooves in vertical sections were not as large as
228 other depressions in fruits (Fig. 3b). Additionally, horizontal grooves near the proximal end might be missing from
229 the samples harvested at 0 and 2 WAB because those samples had peduncles when scanned. Fig. 3c shows the
230 chronological change in horizontal groove point angles, which represented the location of horizontal grooves, for
231 fruit from eight cultivars, as classified by Euclidean distance. Generally, the score increased as the fruit grew, which
232 indicated that horizontal groove positions tended to move from the proximal to the distal end. In particular, 'Tamopan,'
233 which has an "extremely big" horizontal groove (Fruit Tree Experiment Station of Hiroshima Prefecture, 1979), had
234 a distinctive pattern of groove development; the groove position kept changing toward the distal end throughout fruit
235 development. However, 'Kikuhira' and 'Mizushimagosho' did not show any significant differences in groove position

236 since horizontal groove emergence. Groove development became stable at 10 WAB in 'Tenpougai,' 'Midai,' 'Nagara,'
237 and 'Fudegaki,' and at 12 WAB in 'Sakata' (Supplementary Fig. 4).
238 Additionally, changes in horizontal groove depth were also evaluated in 'Tenpougai' and 'Tamopan.' The
239 depth continued to increase from anthesis, but the increase suspended at mid-growth and showed double-sigmoid
240 curve patterns (Fig. 3d). Fruit volume analysis in 'Tamopan' showed that the distal portion, which was beneath the
241 groove, exhibited a double sigmoid-like curve, but the proximal portion, which was above the groove, did not follow
242 this pattern and continued to develop (Fig. 3e). Besides, the volume increase ratio was larger in the proximal portion
243 than in the distal portion throughout the developmental stages except at 20 WAB. Especially in the early growing
244 period, the differences were much larger (Fig. 3e).
245
246 *Developmental analysis of vertical groove variation*
247 In this study, we conducted an in-depth analysis of the genetic diversity of vertical grooves that many
248 cultivars possess. Persimmon generally have four carpels, and vertical grooves develop at carpel fusion zones (Fig.
249 4a). Most persimmon cultivars show various degrees of a vertical groove at anthesis, regardless of vertical groove
250 presence or absence at maturity (Fig. 2c). However, the groove depth can become shallower during development
251 depending on genotype (Fig. 4b).
252 To test if the groove depth is primarily determined by cell division or cell expansion, groove development
253 for ovarian tissues was characterized before and at anthesis in four cultivars with various groove depths. At
254 approximately 3 weeks before anthesis, groove lines were visible along the carpel fusion lines in 'Amayotsumizo'
255 and 'Mizushimagosho,' but not in 'Fuyuu' (Fig. 4c). Microscopic analysis revealed no significant difference between
256 cell sizes in groove-present and -absent zones regardless of the cell types and cultivars except tannin cell size in
257 'Saijou'. However, there was a significant increase in the whole cell numbers counted for both tannin cells and
258 parenchyma cells in groove-absent tissue compared with groove-present tissue in all cultivars (Fig. 4-f; $p < 0.01$ in
259 the paired Student's *t*-test). The significant difference in parenchyma cell number between groove-present and -
260 absence was observed in all four cultivars (Supplementary Fig. 5; $p < 0.01$ in the paired Student's *t*-test). In addition,
261 a significant difference in tannin cell number was also observed in 'Saijou' and 'Amayotsumizo' (Supplementary Fig.

262 5; $p < 0.05$ in the paired Student's *t*-test). These results indicated that vertical groove formation at anthesis is driven
263 by the variations in cell layers of fruit flesh, mainly of parenchyma tissues, rather than differences in cell size.

264 We further characterized molecular genetic regulation of vertical groove development using a
265 transcriptomic approach. In differential expression analysis, genetic variation was categorically incorporated into the
266 multi-factor model to standardize differences in the genetic background among cultivars. The differential expression
267 analysis identified 1,883 DEGs between grooved and non-grooved zones in groove-present cultivars. DEGs were
268 typically enriched for functions in cell wall development and cell fate determination (Table 2). To search for candidate
269 regulators, we identified the lowest q-values, which yielded genes with typical functions in fruit development, such
270 as cell wall-related genes and well-characterized transcription factors (Table 3). Specifically, *SVP* and *YABBY*
271 homologs were among the top 20 DEGs with the lowest q-values (Table 3).

272 *SVP* is a MADS-box factor that determines floral meristem identity (Gregis et al., 2008). The diploid
273 *Diospyros* reference genome has two *SVP* homologs (Supplementary Fig. 6). One *SVP* homolog
274 (evm.model.original_scaffold_495.37), *DkSVP1*, was the DEG with the second lowest q-value among all genes and
275 showed lower expression in groove than non-groove tissue in groove-present cultivars (Supplementary Fig. 6). The
276 same expression pattern was found in groove-absent cultivars. Interestingly, the other *SVP* homolog, *DkSVP2*
277 (evm.model.original_scaffold_1207.202), generally showed opposite expression compared with *DkSVP1*: there was
278 higher expression in groove than in non-groove tissues.

279 The *YABBY* gene family is a central regulator of carpel development. In *Arabidopsis*, *YAB1* and *YAB3* are
280 known to have roles in carpel fusion development (Nole-Wilson and Krizek, 2006). The DEGs highly associated with
281 groove development, evm.model.original_scaffold_883.29 and evm.model.original_scaffold_1133.35 (*DkYABBY1a*
282 and *DkYABBY1c*, respectively), were found in the YAB1/YAB3 clade (Supplementary Fig. 7). *DkYABBY1a* and
283 *DkYABBY1c* expression patterns matched the patterns of groove development and genetic variation. They were
284 significantly more expressed in the grooved zone in most groove-present cultivars, and the mean expression level
285 was higher in cultivars with deeper vertical grooves ('Saijou' and 'Amayotsumizo'); however, there were no
286 significant differences between tissues in the groove-absent cultivars (Fig 5c). Similar expression patterns were also
287 observed in evm.model.fragScaff_scaffold_45.107 (*DkYABBY5a*) and evm.model.original_scaffold_1639.203.1

288 (*DkYABBY1b*) (Supplementary Fig. 7).

289 The functions and expression patterns of *YABBY* family genes explained the groove depth variation.
290 Therefore, we further characterized the associated gene networks (Fig. 5d and Supplementary Fig. 8). Genes with
291 first-degree interactions with *YABBY* genes did not include transcription factors. However, many transporter genes
292 and enzyme-coding genes were found, such as *CYP77A4*, which functions in auxin-mediated patterning (Kawade et
293 al., 2018), and *CYP86A8*, which functions in omega-hydroxylation of various fatty acids during development
294 (Wellesen et al., 2008). Collectively, these results identify the *YABBY* family as a potential molecular factor that
295 directly regulates vertical groove development.

296

297

298 **Discussion**

299 *Utilizing 3D scan for geometric phenotyping of fruit*

300 This study showed that 3D models developed by a 3D scanner captured detailed morphological features of
301 persimmon fruit. In particular, fine characteristics of complex features, such as horizontal and vertical grooves, were
302 clearly reproduced (Fig. 1c and 3b). Conventional persimmon fruit phenotyping was previously conducted based on
303 2D imaging (Maeda et al., 2018, 2019; Kusumi et al., 2022), which did not capture all shape attribute information.
304 In this study, we obtained morphological information along various axes. For example, vertical grooves are more
305 prominent near the proximal or the distal end in some cultivars, but they are more noticeable in the middle portion of
306 the fruit in other cultivars. However, 2D imaging cannot capture grooves that form near the distal end because it is
307 obscured when imaged from one side of the fruit. In addition, the horizontal grooves do not typically cover the entire
308 fruit circumference, which results in loss of information when conducting 2D imaging. To address these issues, we
309 used a 3D modeling approach that allowed us to integrate information from multiple sections along the proximal–
310 distal line.

311

312 *3D modeling clarifies complex shape development in persimmon fruit*

313 In this study, we observed that the vertical groove depth decreased during growth stage 1, with variations

depending on genotype. However, all cultivars had vertical grooves at anthesis, but with differing depths (Fig. 2). Therefore, it was suggested that the formation of vertical grooves occurred during carpel fusion, and the groove pattern at maturity is shaped by combination of the fusion pattern and cell growth patterns after formation, which could be mainly driven by cell divisions.

On the other hand, the results indicated that horizontal groove development in persimmon fruit is promoted by the different growth speeds between fruit portions above and beneath the groove. We observed that the horizontal groove position shifted toward the distal end and the groove continued to deepen throughout fruit development, which could be attributed to vertical growth and horizontal growth, respectively (Fig. 3c and 3d). This demonstrates that both vertical and horizontal development speeds of proximal tissues above the groove were much faster than those of the distal tissue during early fruit growth, and became similar around growth stages 2-3 depending on cultivars (Fig. 3e and 3f). These observations are consistent with the findings of previous studies, which reported that growth at the proximal end in persimmon fruit is more vigorous during stage 1, which could continue until early-mid August (Fujimura, 1935). Collectively, we showed that differences in the horizontal and vertical growth speeds between portions of the fruit, divided by the horizontal groove, explained horizontal groove development and movement of its position (Fig. 3f).

Maeda et al. (2018) reported that fruit L/W ratio was the main contributor to shape variation in longitudinal fruit sections based on PCA of diverse persimmon cultivars. They found that the correlation coefficients between PC1, which represented L/W ratio variability, at maturity and that of several different developmental stages reached 0.9 at the end of June. In this experiment, correlation analysis was conducted between the L/W ratio at maturity and that of different developmental stages. The correlation coefficient reached at 0.9 between 4–6 WAB (Supplementary Fig. 3b). This result was also consistent with that of Sugiura et al. (1977), in which ethanol treatment of persimmon fruits after flowering until late July influenced the fruit L/W ratio. In this study, we further showed that each genotype had variable transitions; the period for determining L/W ratio varied from 0 WAB to maturity depending on cultivar (Table 1). In addition, we found that the L/W ratio was determined later in cultivars with oblong fruit, such as ‘Fudegaki’ or ‘Nagara.’ This probably means that vertical cell division or expansion receive more resources in oblong cultivars, which causes slower transverse development, but horizontal and vertical development can become equal

340 earlier in other cultivars.

341

342 *Cell identity control is the most likely mechanism underlying vertical groove development variation*

343 Vertical grooves in fruit are known to emerge in many species, including *Cucumis* and *Prunus* (Paris, 2016;
344 Yousif et al., 2011). Multiple genetic studies have explored the genes that contribute to groove formation, but the
345 molecular mechanism of their development is not fully understood. Yao et al. (2018) found that overexpression of
346 *Malus domestica PISTILLATA* causes vertical groove development on fruit from 12 days after pollination. Du et al.
347 (2022) identified a 1.07-kb deletion of a chromosome segment in groove lines of *Cucumis melo* and proposed that
348 *CmMADS-Box* may be a candidate gene regulating the groove formation. It was also reported that certain *Arabidopsis*
349 mutants with defects in the *YABBY* and *SVP* genes produced flowers with abnormal carpel fusions, which can possibly
350 lead to groove-like structures (Nole-Wilson and Krizek, 2006; Gregis et al., 2009). However, there has been no report
351 to date of *YABBY* or *SVP* directly regulating groove formation in species with fleshy fruit.

352 Our transcriptome analysis indicated that DEGs between grooved and non-grooved zones were related to
353 cell wall development or cell fate, which is consistent with the observation that grooves were formed by fewer cell
354 layers at carpel margins (Fig. 4). Interestingly, of the DEGs, *SVP* and *YABBY* gene families had low q-values (Table
355 3). *SVP* is known to be involved in determination of floral organ identity in *Arabidopsis* and tomato (Liu et al., 2007;
356 Thouet et al., 2012). However, *YABBY* controls establishment of abaxial–adaxial polarity in lateral organs (van der
357 Knapp et al., 2014). *YABBY* is a plant-specific transcription factor with several family members (Bowman, 2000);
358 *FIL* and *YAB3* define the abaxial cell fate in lateral organs in *Arabidopsis* (Siegfried et al., 1999). Besides, *YAB2* and
359 *YAB5*, which are expressed specifically in the abaxial side, can also contribute to the polarity formation with less
360 magnificent effect (Stahle et al., 2009; Sarojam et al., 2010). Importantly, *DkSVP1* expression was also high in
361 groove-absent cultivars, whereas *DkYABBY1a* and *DkYABBY1c* expression completely matched the groove patterns,
362 including presence/absence among different cultivars (Fig 5c). These results strongly suggest that *YABBY* homologs
363 are direct regulators of vertical groove development.

364 The gene co-expression network of *DkYABBY1a/1c* did not include any transcription factors, which
365 indicated that *YABBY*s are upstream regulators of the network (Fig. 5d). Most genes associated with *YABBY*s are

366 transporters and enzymes, and they seemed to be functionally related to cell development. In particular, enzymes
367 related to hydrocarbon metabolism were highly enriched, such as cytochrome P450 proteins (Fukushima et al., 2011)
368 and lipolytic enzymes. *CYP77A4* was reported to be involved in establishing polarity in *A. thaliana* embryos by
369 regulating auxin distribution pattern; thus, it plays an important role in leaf morphogenesis (Kawade et al., 2018).
370 Additionally, pectate lyase was found in the network, which helps cell wall remodeling (Uluisik and Seymour, 2020).
371 Considering the expression pattern, biological function in model species, and co-expression network, it is very likely
372 that the *YABBY* homologs directly regulate vertical groove development. It should be noted that multiple *YABBY*
373 homologs were expressed in a highly correlated manner, which indicates an additional layer of expression regulation
374 underlying the genetic variation in vertical groove development. Further functional analysis, including examination
375 of characteristic paralogs, in persimmon may offer new insights into this process.
376
377
378 **Acknowledgments**
379 We thank Mallory Eckstut, PhD, from Edanz (https://jp.edanz.com/ac) for editing a draft of this manuscript.
380 This work was supported by the Japan Society for the Promotion of Science KAKENHI Grant Number 20K20454 to
381 SN and RT, and 21KK0269 to SN.
382
383 **References**
384 Bowman, J.L. 2000. The *YABBY* gene family and abaxial cell fate. Curr. Opin. Plant Biol. 3：17-22.
385 Bradski, G. 2000. The OpenCV Library. Dr. Dobb's j. softw. tools prof. program. 25: 120-123.
386 Chen, S., Y. Zhou, Y. Chen and J. Gu. 2018. Fastp: An ultra-fast all-in-one FASTQ preprocessor. Bioinformatics. 34:
387 i884–i890.
388 Cignoni, P., M. Callieri, M. Corsini, M. Dellepiane, F. Ganovelli and G. Ranzuglia. 2008. MeshLab: an Open-Source
389 Mesh Processing Tool. Sixth Eurographics Italian Chapter Conference.129-136
390 Cliff, M., K. Sanford, W. Wismer and C. Hampson. 2002. Use of digital images for evaluation of factors responsible
391 for visual preference of apples by consumers. HortScience. 37: 1127-1131

392 Cong, B., L.S. Barrero and S.D. Tanksley. 2008. Regulatory change in *YABBY*-like transcription factor led to
393 evolution of extreme fruit size during tomato domestication. Nat. Genet. 40:800–804.
394 Currie, A.J., S. Ganeshanandam, D.A. Noiton, D. Garrick, C.J.A. Shelbourne and N. Oraguzie. 2000. Quantitative
395 evaluation of apple (*Malus* × *domestica* Borkh.) fruit shape by principal component analysis of Fourier
396 descriptors, Euphytica. 111: 221-227
397 Ding, W., Nesumi, H., Yamada, M., Takano, Y., 2000. Quantitative evaluation of 3-dimentional fruit morphology and
398 its applications to genetic analysis. Jpn. J. Biomet. 20, 131-141, in Japanese with English abstract.
399 Dobin, A., C.A. Davis, F. Schlesinger, J. Drenkow, C. Zaleski, S. Jha, P. Batut, M. Chaisson and T.R. Gingeras. 2013.
400 STAR: Ultrafast universal RNA-seq aligner. Bioinformatics 29:15–21.
401 Du, X., H. Liu, Z. Zhu, S. Liu, Z. Song, L. Xia, J. Zhao, F. Luan and S. Liu. 2022. Identification of candidate
402 chromosome region related to melon (*Cucumis melo* l.) fruit surface groove trait through biparental genetic
403 mapping and genome-wide association study. Front. Plant Sci. 13.
404 Ferrándiz, C., C. Fourquin, N. Prunet, C.P. Scutt, E. Sundberg, C. Trehin, A. Lie and C.M. Vialette-Guiraud. 2010.
405 Carpel Development. Adv. Bot. Res. 55: 1-73
406 Fruit Tree Experiment Station of Hiroshima Prefecture. 1979. Showa 53-nendo Shubyo-tokusei-bunrui-chosa-
407 hokokusho (Kaki). Fruit Tree Experiment Station of Hiroshima Prefecture, Hiroshima, Japan. In Japanese.
408 Fujimura, J. 1935. The research on persimmon fruit development. J. Jpn. Soc. Hortic. Sci. 6: 105-117. In Japanese.
409 Fukushima, E.O., H. Seki, K. Ohyama, E. Ono, N. Umemoto, M. Mizutani, K. Saito and T. Muranaka. 2011.
410 *CYP716A* subfamily members are multifunctional oxidases in triterpenoid biosynthesis. Plant Cell Physiol.
411 52:2050–2061.
412 Gillaspy, G., H. Ben-David and W. Gruissem. 1993. Fruits: a developmental perspective, The Plant Cell. 5: 1439-
413 1451.
414 Gonzalo, M.J., M.T. Brewer, C. Anderson, D. Sullivan, S. Gray and E. van der Knaap. 2009. Tomato fruit shape
415 analysis using morphometric and morphology attributes implemented in Tomato Analyzer software program. J.
416 Am. Soc. Hortic. 134: 77-87
417 Gregis, V., A. Sessa, L. Colombo and M.M. Kater. 2008. *AGAMOUS-LIKE24* and *SHORT VEGETATIVE PHASE*

determine floral meristem identity in Arabidopsis. Plant Journal 56:891–902.

He, J.Q., R.J. Harrison and B. Li. 2017. A novel 3D imaging system for strawberry phenotyping. Plant Methods. 13.

Honma, T and K. Goto. 2001. Complexes of MADS-box proteins are sufficient to convert leaves into floral organs. Nature. 409: 525–529

Howe, H.F. and J. Smallwood. 1982. Ecology of Seed Dispersal, Source: Annual Review of Ecology and Systematics. 13: 201-228

Huerta-Cepas, J., D. Szklarczyk, D. Heller, A. Hernández-Plaza, S.K. Forslund, H. Cook, D.R. Mende, I. Letunic, T. Rattei, L.J. Jensen, C. von Mering and P. Bork. 2019. EggNOG 5.0: A hierarchical, functionally and phylogenetically annotated orthology resource based on 5090 organisms and 2502 viruses. Nucleic Acids Res. 47: D309–D314.

Kawade, K., Y. Li, H. Koga, Y. Sawada, M. Okamoto, A. Kuwahara, H. Tsukaya and M.Y. Hirai. 2018. The cytochrome P450 CYP77A4 is involved in auxin-mediated patterning of the Arabidopsis thaliana embryo. Development. 145.

Kawamoto, T. 1990. Light microscopic autoradiography for study of early changes in the distribution of water-soluble materials. J. Histochem. Cytochem. 38: 1805-1814.

van der Knaap, E., M. Chakrabarti, Y.H. Chu, J.P. Clevenger, E. Illa-Berenguer, Z. Huang, N. Keyhaninejad, Q. Mu, L. Sun, Y. Wang and S. Wu. 2014. What lies beyond the eye: the molecular mechanisms regulating tomato fruit weight and shape. Front. Plant Sci. 5:227

Kusumi, A., Y. Osako, R. Nakano, S. Nishiyama and R. Tao. 2022. Phenotypic evaluation of shape diversity in persimmon fruit using two- and three-dimensional imaging. Acta Horticulturae. International Society for Horticultural Science: 263-268.

Langfelder, P. and S. Horvath. 2008. WGCNA: An R package for weighted correlation network analysis. BMC Bioinformatics 9.

Li, H., B. Handsaker, A. Wysoker, T. Fennell, J. Ruan, N. Homer, G. Marth, G. Abecasis and R. Durbin. 2009. The sequence alignment/map format and SAMtools. Bioinformatics. 25: 2078-2079.

Li, M., M.R. Shao, D. Zeng, T. Ju, E.A. Kellogg and C.N. Topp. 2020. Comprehensive 3D phenotyping reveals

444 continuous morphological variation across genetically diverse sorghum inflorescences. New Phytol. 226: 1873-
445 1885.
446 Liu, C., J. Zhou, K. Bracha-Drori, S. Yalovsky, T. Ito and H. Yu. 2007. Specification of *Arabidopsis* floral meristem
447 identity by repression of flowering time genes. Development 134:1901–1910.
448 Liu, J., X. Xu, Y. Liu, Z. Rao, M.L. Smith, L. Jin and B. Li. 2021. Quantitative potato tuber phenotyping by 3D
449 imaging. Biosyst. Eng. 210:48–59.
450 Love MI, W. Huber and S. Anders. 2014. Moderated estimation of fold change and dispersion for RNA-seq data with
451 DESeq2. Genome Biol. 15: 550.
452 Maeda, H., T. Akagi and R. Tao. 2018. Quantitative characterization of fruit shape and its differentiation pattern in
453 diverse persimmon (*Diospyros kaki*) cultivars. Sci. Hortic. 228:41–48.
454 Maeda, H., T. Akagi, N. Onoue, A. Kono, and R. Tao, Evolution of lineage-specific gene networks underlying the
455 considerable fruit shape diversity in persimmon. Plant Cell Physiol. 60:2464–2477
456 Magnus Eklund, D., V. Ståldal, I. Valsecchi, I. Cierlik, C. Eriksson, K. Hiratsu, M. Ohme-Takagi, J.F. Sundström, M.
457 Thelander, I. Ezcurra and E. Sundberg. 2010. The *Arabidopsis thaliana* STYLISH1 protein acts as a
458 transcriptional activator regulating auxin biosynthesis. Plant Cell 22:349–363.
459 Mezzetti, B., L. Landi, T. Pandolfini and A. Spena. 2004. The *defH9-iaaM* auxin-synthesizing gene increases plant
460 fecundity and fruit production in strawberry and raspberry BMC Biotechnol. 4:4.
461 Nii, N. 1980. Seasonal changes of fruit growth in Japanese persimmon, *Diospyros kaki* cv. Fuyu, in relation to
462 vascular tissue development in the fruit stalk. J. Jpn. Soc. Hortic. Sci. 49: 160-170.
463 Nishiyama, S. and H. Yamane. 2022. Fruit-Size Control. In: The Persimmon Genome: Springer, Cham. p. 155–165.
464 Nole-Wilson, S. and B.A. Krizek. 2006. AINTEGUMENTA contributes to organ polarity and regulates growth of
465 lateral organs in combination with YABBY genes. Plant Physiol. 141:977–987.
466 Onoue, N., S. Kobayashi, A. Kono and A. Sato. 2018. SSR-based molecular profiling of 237 persimmon (*Diospyros*
467 *kaki* Thunb.) germplasms using an ASTRINGENCY-linked marker. Tree Genet. Genomes 14: 1-18.
468 Osako, Y., H. Yamane, S.Y. Lin, P.A. Chen and R. Tao. 2020. Cultivar discrimination of litchi fruit images using deep
469 learning. Sci. Hortic. 269.

470 Paris, H.S. 2016. Germplasm enhancement of *Cucurbita pepo* (pumpkin, squash, gourd: Cucurbitaceae): progress
471 and challenges. Euphytica. 208: 415-438.
472 Putri, G.H., S. Anders, P.T. Pyl, J.E. Pimanda and F. Zanini. 2022. Analysing high-throughput sequencing data in
473 Python with HTSeq 2.0. Bioinformatics 38:2943–2945.
474 Sarojam, R., P.G. Sappl, A. Goldshmidt, I. Efroni, S.K. Floyd, Y. Eshed and J.L. Bowman. 2010. Differentiating
475 Arabidopsis shoots from leaves by combined YABBY activities. The Plant Cell. 22: 2113-2130.
476 Scutt, C.P., M. Vinauger-Douard, C. Fourquin, C. Finet and C. Dumas. 2006. An evolutionary perspective on the
477 regulation of carpel development. J. Exp. Bot. 57: 2143-2152.
478 Seymour, G.B., L. Ostergaard, N.H. Chapman, S. Knapp and C. Martin. 2013. Fruit development and ripening. Annu.
479 Rev. Plant Biol.
480 Shimomura, K., H. Horie, M. Sugiyama, Y. Kawazu and Y. Yoshioka. 2016. Quantitative evaluation of cucumber
481 fruit texture and shape traits reveals extensive diversity and differentiation. Sci. Hortic. 199:133–141.
482 Siegfried, K.R., Y. Eshed, S.F. Baum, D. Otsuga, G.N. Drews and J.L. Bowman. 1999. Members of the *YABBY* gene
483 family specify abaxial cell fate in *Arabidopsis*. Development. 126: 4117-4128.
484 Stahle, M.I., J. Kuehlich, L. Staron, A.G. von Arnim and J.F. Golz. 2009. YABBYs and the transcriptional
485 corepressors LEUNIG and LEUNIG_HOMOLOG maintain leaf polarity and meristem activity in *Arabidopsis*.
486 The Plant Cell. 21: 3105-3118.
487 Suo, Y., P. Sun, H. Cheng, W. Han, S. Diao, H. Li, Y. Mai, X. Zhao, F. Li and J. Fu. 2020. A high-quality chromosomal
488 genome assembly of *Diospyros oleifera* Cheng. Gigascience 9.
489 Sugiura, A., H. Harada and T. Tomana. 1977. Studies on the removal of astringency in Japanese persimmon fruits Ⅱ.
490 on-tree removal of astringency by ethanol treatment (Part II). J. Jpn. Soc. Hortic. Sci. 46: 303-309 in Japanese
491 with English abstract.
492 Thouet, J., M. Quinet, S. Lutts, J.M. Kinet and C. Périlleux. 2012. Repression of floral meristem fate is crucial in
493 shaping tomato inflorescence. PLoS One 7.
494 Uluisik, S. and G.B. Seymour. 2020. Pectate lyases: Their role in plants and importance in fruit ripening. Food Chem.
495 309: 125559.

496 UPOV. 2004. TG/92/4 Persimmon, 2004-03-31. Guidelines for conduct of tests for distinctness, homogeneity and
497 stability −persimmon (*Diospyros kaki* L.). Geneva. International Union for the protection of new varieties of
498 plants (UPOV).
499 Wan, C.Y. and T. A. Wilkins. 1994. A modified hot borate method significantly enhances the yield of high-quality
500 RNA from cotton (*Gossypium hirsutum* L.). Anal. Biochem. 223: 7-12.
501 Wellesen, K., F. Durst, F. Pinot, I. Benveniste, K. Nettesheim, E. Wisman, S. Steiner-Lange, H. Saedler and A.
502 Yephremov. 2001. Functional analysis of the *LACERATA* gene of *Arabidopsis* provides evidence for different
503 roles of fatty acid ω-hydroxylation in development. Proc. Natl. Acad. Sci. U.S.A. 98:9694-9699.
504 Yao, J.L., J. Xu, S. Tomes, W. Cui, Z. Luo, C. Deng, H.S. Ireland, R.J. Schaffer and A.P. Gleave. 2018. Ectopic
505 expression of the *PISTILLATA* homologous *MdPI* inhibits fruit tissue growth and changes fruit shape in apple.
506 Plant Direct 2: e00051.
507 Young, M.D., M.J. Wakefield, G.K. Smyth and A. Oshlack. 2010. Gene ontology analysis for RNA-seq: accounting
508 for selection bias. Genome Biol. 11: 1-12.
509 Yousif, M.T., T.M. Elamin, A. Fadil, M. Baraka, A.A. el Jack and E.A. Ahmed. 2011. Variability and correlation
510 among morphological, vegetative, fruit and yield parameters of snake melon (*Cucumis Melo* Var. Flexuosus).
511 Cucurbit Genet. Coop. Report. 33: 32-35.
512

513 **Conflict of Interest**

514 The authors declare no conflict of interest.

515

516

517 **Figure legends**

518 **Figure 1. Three-dimensional scanning of fruit from diverse persimmon cultivars.** (a, b) Diversity of (a) vertical
519 and (b) horizontal grooves in persimmon fruits. (c) An example of self-occlusions in 'Gobangaki.' (d) 3D model of
520 'Ooniwa' at maturity. (e) Horizontal sections of 3D models. Scores and descriptors in (a) and (b) are based on Fruit
521 Tree Experiment Station of Hiroshima Prefecture (1979).

522 **Figure 2. Characterization of vertical groove development.** (a) Schematic of the measurement method used to
523 determine groove index (GI). (b) Transition of GI in 'Ooniwa' throughout developmental stages. (c) Heatmap of the
524 transition of GI#20-89, with asterisks indicating cultivars classified as having vertical grooves by Fruit Tree
525 Experiment Station of Hiroshima Prefecture (1979) and visually verified when no recorded reference was available.

526 **Figure 3. Characterization of horizontal groove development.** (a) Schematic of the measurement method used to
527 determine horizontal grooves. (b) 3D models of (i) 'Kikuhira,' (ii) 'Nagara,' (iii) 'Sakata,' (iv) 'Fudegaki,' (v)
528 'Tenpougai,' (vi) 'Tamopan,' (vii) 'Midai,' and (viii) 'Mizushimagosho.' (c) Heatmap of the transition of groove
529 position (angle between line A and line B in Figure 3a). (d) Transition patterns of groove depth in 'Tenpougai' and
530 'Tamopan.' The black line indicates the horizontal groove depth. (e) Transition of volume and volume increase ratio
531 in 'Tamopan.' (f) Proposed developmental model for horizontal grooves.

532 **Figure 4. Morphological characterization of groove tissue.** (a) 3D model of 'Gionbou' at anthesis showing grooves
533 at the boundaries of the fused carpels. (b) Chronological change of groove development in 'Gionbou.' (c) Ovaries of
534 (i) 'Amayotsumizo,' (ii) 'Mizushimagosho,' and (iii) 'Fuyuu' at three weeks before anthesis (23 April 2022). Black
535 arrowheads indicated grooving lines. (d) Measurement of cell number and area in the grooved and non-grooved zones
536 using baselines set at the tip of developing seeds. (e) Microscopy analysis performed on grooved and non-grooved
537 zones for four cultivars. MIZ, SAI, AMA, and FUY represent 'Mizushimagosho,' 'Saijou,' 'Amayotsumizo,' and
538 'Fuyuu,' respectively. Blue-dyed cells are tannin cells. (f) Comparison of parenchyma cell size, tannin cell size, and
539 cell layers measured in each zone (grooved, G, and non-grooved, N) in four cultivars. Single and double asterisks
540 indicate significant differences by paired t-test at $p < 0.05$ and $p < 0.01$, respectively.

541 **Figure 5. Transcriptome analysis of vertical groove development.** (a) Grooved (G) and non-grooved (N) zones
542 from which RNA was extracted. (b) Vertical groove depths at 4 and 20 WAB. (c) Expression patterns of *DkYABBY1a*

543 and *DkYABBY1c*. (d) Gene co-expression network for *DkYABBY1a*/*1c*. The full network of this module is presented

544 in Supplementary Figure S8. ZEN, FUY, FUJ, IWA, GIO, MIZ, SAI, and AMA represent ‘Zenjimaru,’ ‘Fuyuu,’ ‘Fuji,’

545 ‘Iwasedo,’ ‘Gionbou,’ ‘Mizushimagosho,’ ‘Saijou,’ and ‘Amayotsumizo,’ respectively.

546

547

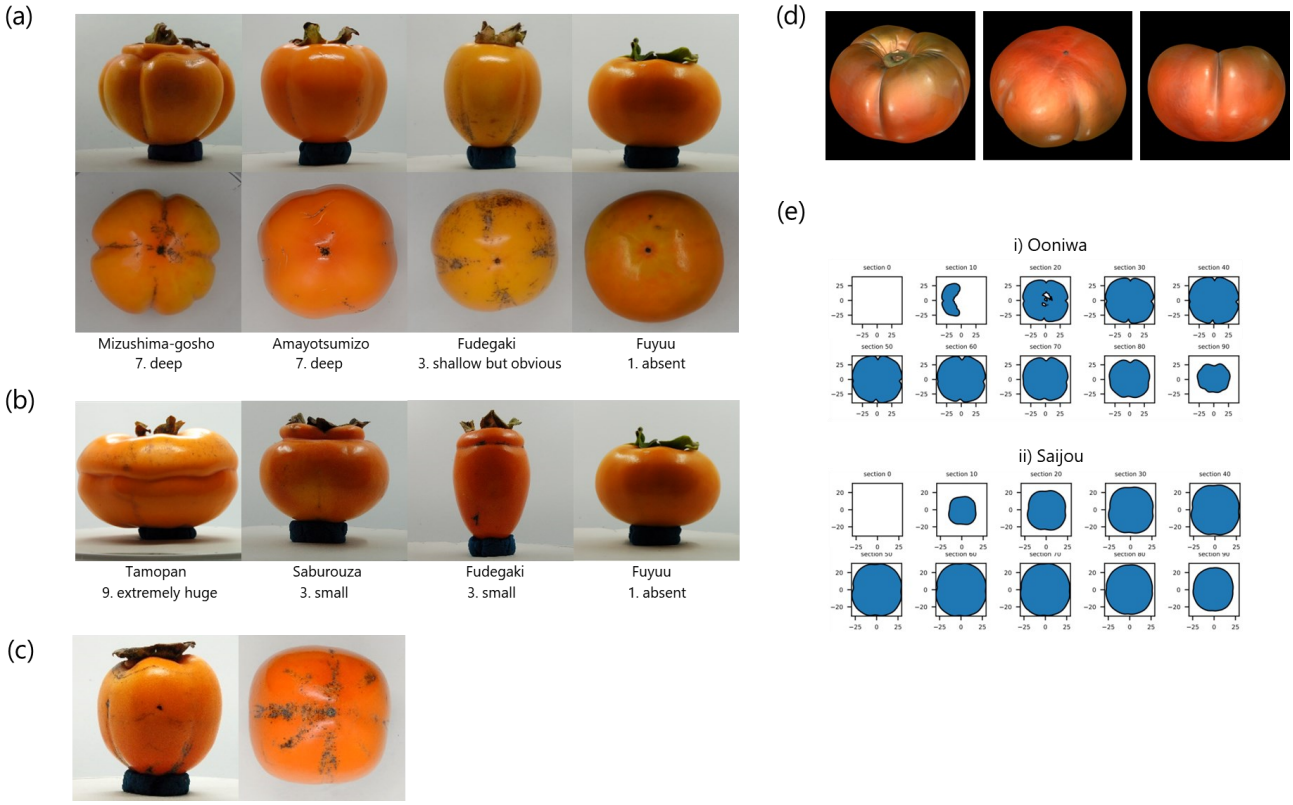

Figure 1. Three-dimensional scanning of fruit from diverse persimmon cultivars. (a, b) Diversity of (a) vertical and (b) horizontal grooves in persimmon fruits. (c) An example of self-occlusions in ‘Gobangaki.’ (d) 3D model of ‘Ooniwa’ at maturity. (e) Horizontal sections of 3D models. Scores and descriptors in (a) and (b) are based on Fruit Tree Experiment Station of Hiroshima Prefecture (1979).

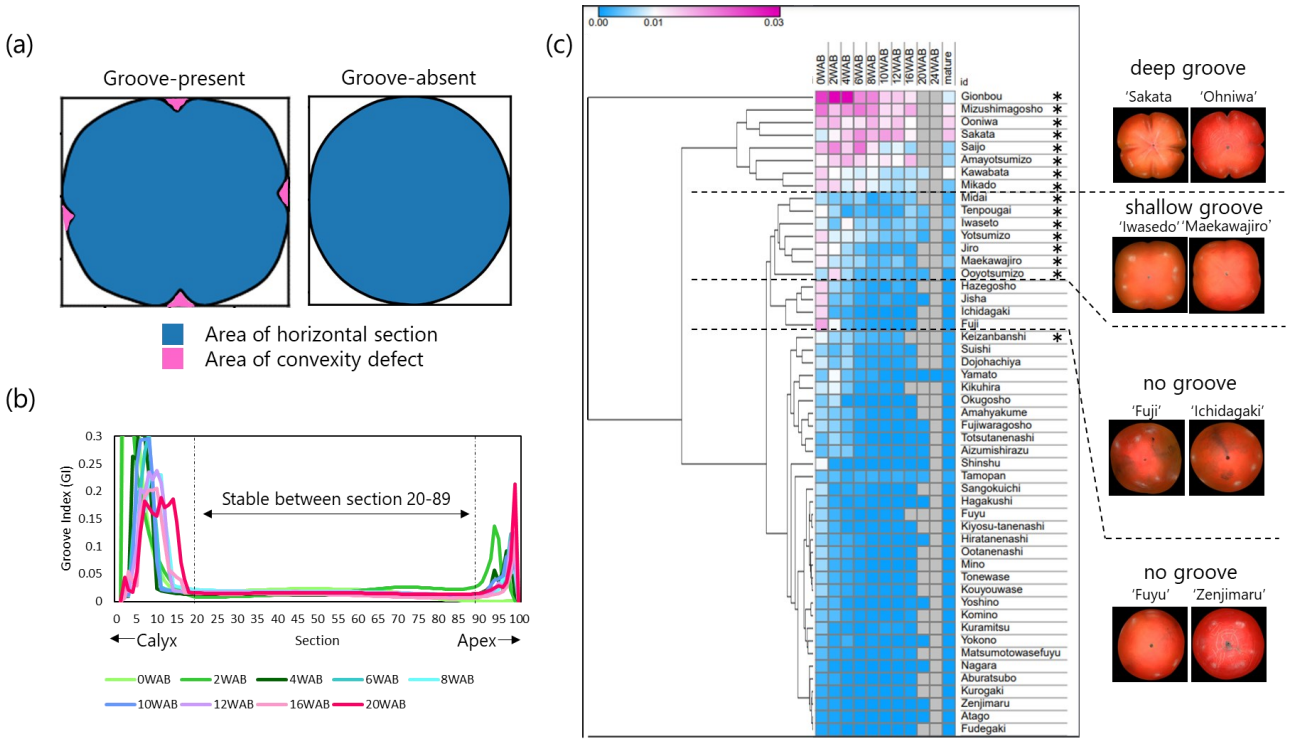

Figure 2. Characterization of vertical groove development. (a) Schematic of the measurement method used to determine groove index (GI). (b) Transition of GI in 'Ooniwa' throughout developmental stages. (c) Heatmap of the transition of GI#20-89, with asterisks indicating cultivars classified as having vertical grooves by Fruit Tree Experiment Station of Hiroshima Prefecture (1979) and visually verified when no recorded reference was available.

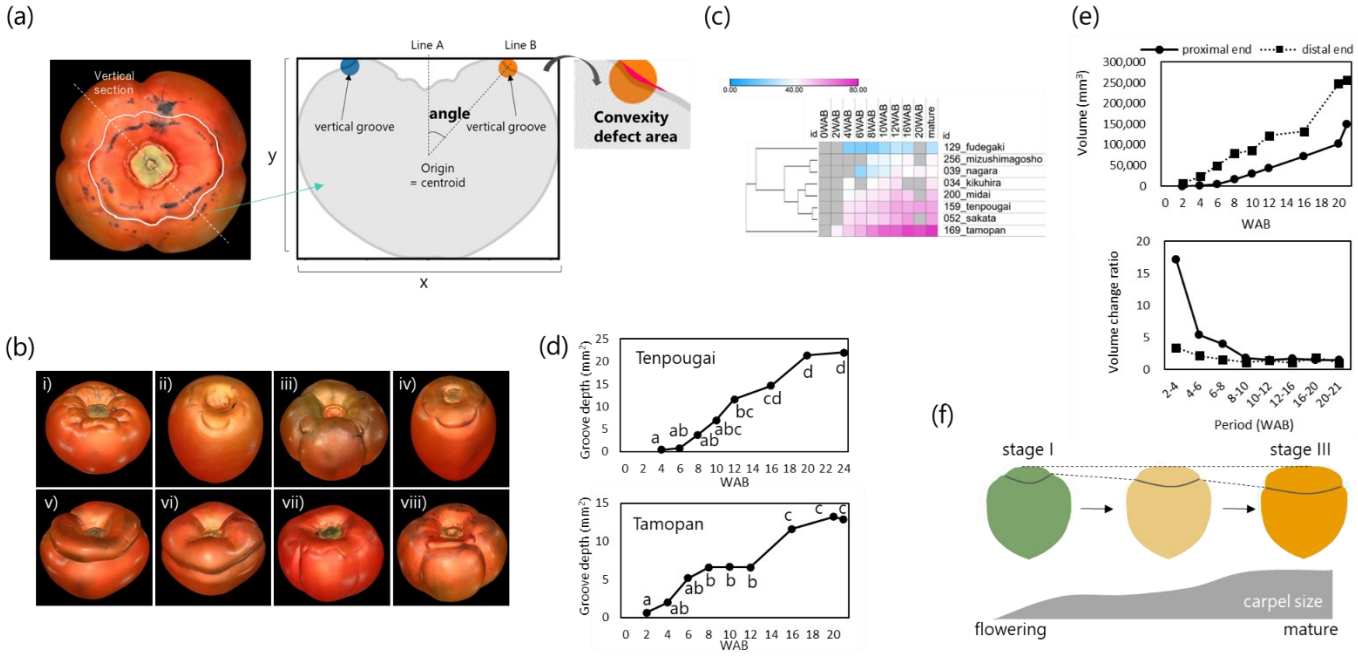

Figure 3. Characterization of horizontal groove development. (a) Schematic of the measurement method used to determine horizontal grooves. (b) 3D models of (i) 'Kikuhira,' (ii) 'Nagara,' (iii) 'Sakata,' (iv) 'Fudegaki,' (v) 'Tenpougai,' (vi) 'Tamopan,' (vii) 'Midai,' and (viii) 'Mizushimagosho.' (c) Heatmap of the transition of groove position (angle between line A and line B in Figure 3a). (d) Transition patterns of groove depth in 'Tenpougai' and 'Tamopan.' The black line indicates the horizontal groove depth. (e) Transition of volume and volume increase ratio in 'Tamopan.' (f) Proposed developmental model for horizontal grooves.

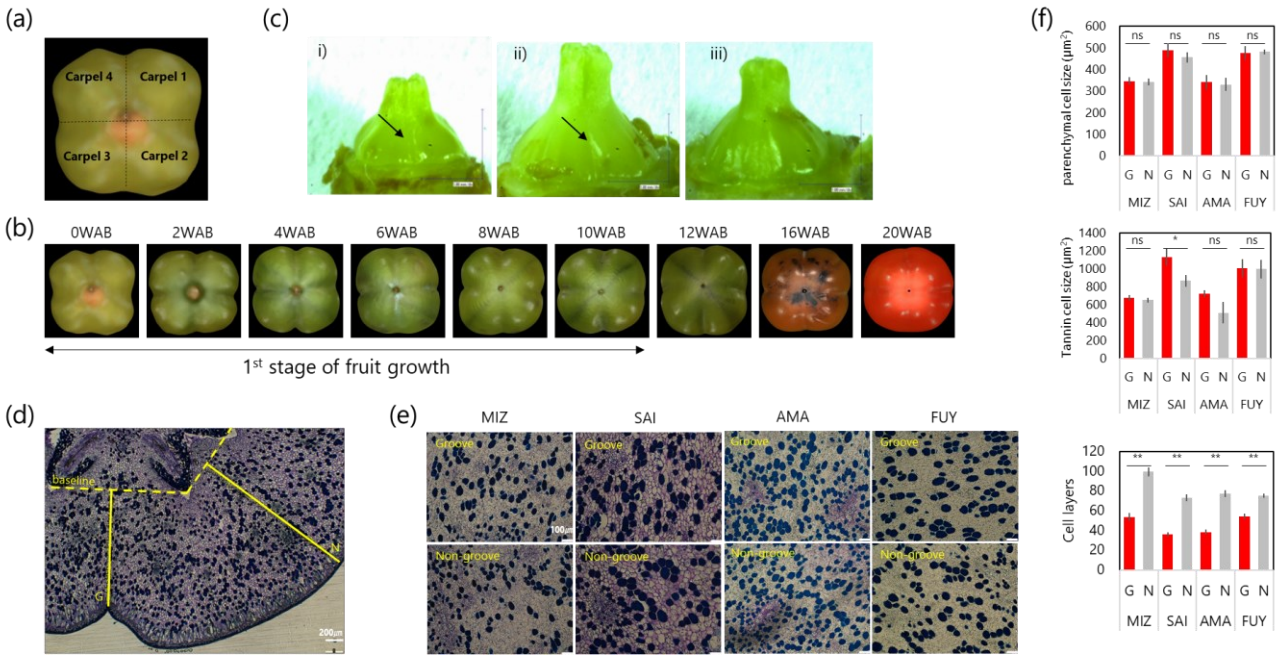

Figure 4. Morphological characterization of groove tissue. (a) 3D model of 'Gionbou' at anthesis showing grooves at the boundaries of the fused carpels. (b) Chronological change of groove development in 'Gionbou.' (c) Ovaries of (i) 'Amayotsumizo,' (ii) 'Mizushimagosho,' and (iii) 'Fuyuu' at three weeks before anthesis (23 April 2022). Black arrowheads indicated grooving lines. (d) Measurement of cell number and area in the grooved and non-grooved zones using baselines set at the tip of developing seeds. (e) Microscopy analysis performed on grooved and non-grooved zones for four cultivars. MIZ, SAI, AMA, and FUY represent 'Mizushimagosho,' 'Saijou,' 'Amayotsumizo,' and 'Fuyuu,' respectively. Blue-dyed cells are tannin cells. (f) Comparison of parenchyma cell size, tannin cell size, and cell layers measured in each zone (grooved, G, and non-grooved, N) in four cultivars. Single and double asterisks indicate significant differences by paired t-test at $p < 0.05$ and $p < 0.01$, respectively.

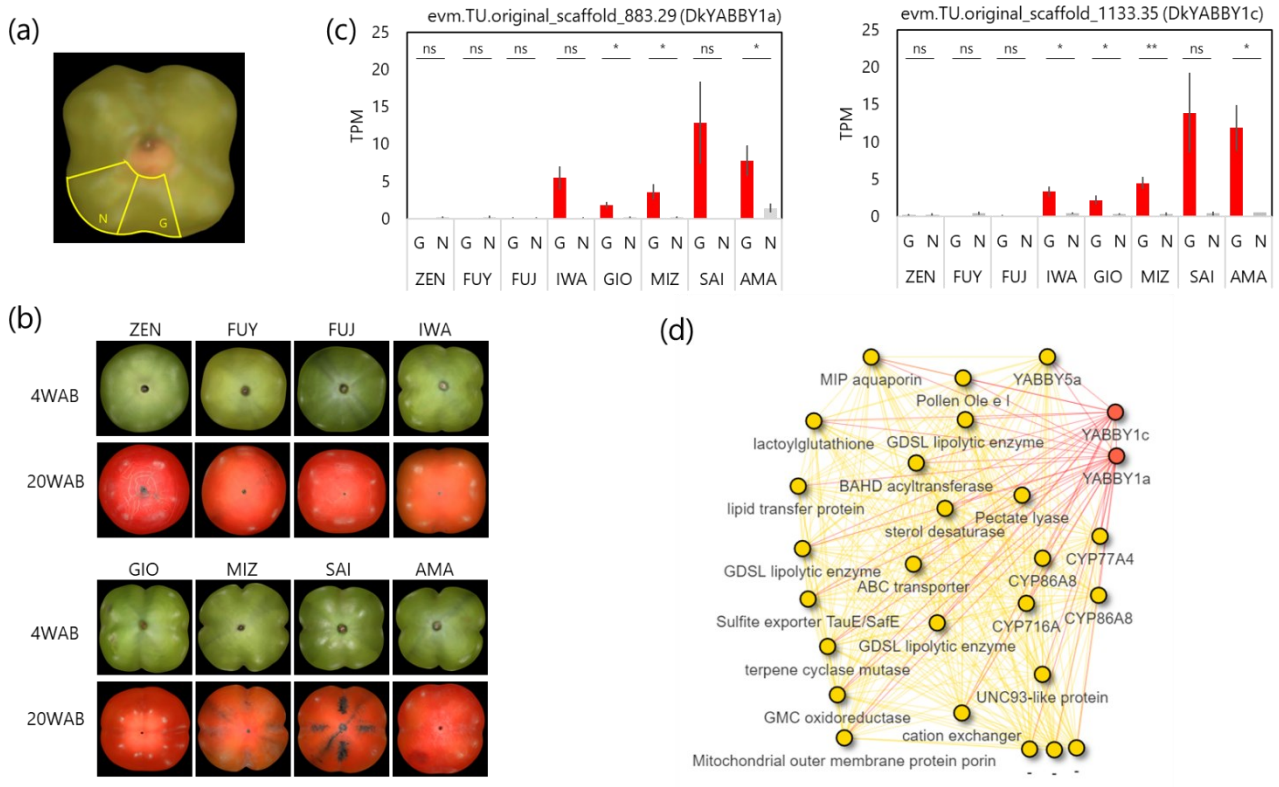

Figure 5. Transcriptome analysis of vertical groove development. (a) Grooved (G) and non-grooved (N) zones from which RNA was extracted. (b) Vertical groove depths at 4 and 20 WAB. (c) Expression patterns of *DkYABBY1a* and *DkYABBY1c*. Single and double asterisks indicate significant differences at $p < 0.05$ and $p < 0.01$ by paired t-test, respectively. (d) Gene co-expression network for *DkYABBY1a*/*1c*. The full network of this module is presented in Supplementary Figure S8. ZEN, FUY, FUJ, IWA, GIO, MIZ, SAI, and AMA represent 'Zenjimaru,' 'Fuyuu,' 'Fuji,' 'Iwasedo,' 'Gionbou,' 'Mizushimagosho,' 'Saijou,' and 'Amayotsumizo,' respectively.

Table 1. Cultivars used in this study.

No.	Cultivar	Vertical groove	Horizontal groove	Determining timing (WAB)				
				GI#20-89	Ro#20-89	L/W	Horizontal groove position	Horizontal groove depth
1	Zenjimaru			2	2	12		
2	Hazegosho			2	6	8		
3	Maekawajiro	*		2	2	4		
4	Kurogaki			4	4	4		
5	Aburatsubo			4	8	at maturity		
6	Amayotsumizo	*		6	4	8		
7	Aizumishirazu			6	6	8		
8	Fujiwaragosho			4	4	4		
9	Kikuhira		*	4	0	4	4	
10	Koyowase			4	6	4		
11	Nagara		*	2	8	at maturity	12	
12	Matsumotowasefuyuu			2	4	2		
13	Totsutanenashi			6	6	6		
14	Shinshuu			2	6	20		
15	Sakata	*	*	0	0	8	12	
16	Tonewase			4	0	6		
17	Atago			4	6	4		
18	Gionbou	*		6	4	8		
19	Kiyosu-tanenashi			4	10	6		
20	Ooyotsumizo	*		6	4	4		
21	Jisha			6	4	8		
22	Ichidagaki			2	8	8		
23	Saijou	*		8	10	at maturity		
24	Dojohachiya			6	0	6		
25	Ootanenashi			4	0	4		
26	Yokono			2	4	8		
27	Fuji			4	4	10		
28	Jirou	*		4	4	0		
29	Yamato			6	10	12		
30	Fudegaki		*	4	4	at maturity	10	
31	Komino			4	6	4		
32	Amahyakume			6	16	16		
33	Okugosho			4	6	10		
34	Mino			2	6	10		
35	Yoshino			4	4	4		
36	Yotsumizo	*		8	2	2		
37	Tenpougai	*	*	2	0	4	10	16
38	Hiratanenashi			6	2	4		
39	Tamopan		*	4	0	0	at maturity	16
40	Fuyuu			4	8	4		
41	Iwasedo	*		6	0	4		
42	Midai	*	*	0	4	4	10	
43	Hagakushi			2	10	10		
44	Sangokuichi			2	0	8		
45	Kuramitsu			2	0	10		
46	Mizugaki/suishi			6	0	8		
47	Ooniwa	*		0	0	8		
48	Kawabata	*		0	0	20		
49	Keizanbanshi	*		2	4	2		
50	Mikado	*		8	4	4		
51	Mizushimagosho	*	*	8	8	4	8	

Asterisks indicates the presence of vertical or horizontal groove.

592 **Table 2. GO enrichment analysis for DEGs**

GO ID	Term	Annotated gene count	gene count in the cluster	Expected count	q-value
GO:0009834	plant-type secondary cell wall biogenesis	24	67	4.13	4.61E-07
GO:0009699	phenylpropanoid biosynthetic process	26	90	5.55	1.18E-05
GO:0009698	phenylpropanoid metabolic process	27	101	6.23	2.88E-05
GO:0042335	cuticle development	15	37	2.28	5.85E-05
GO:0042546	cell wall biogenesis	37	191	11.77	2.19E-04
GO:0009809	lignin biosynthetic process	14	38	2.34	6.37E-04
GO:0048046	apoplast	42	261	16.09	8.98E-04
GO:0045491	xylan metabolic process	16	53	3.27	1.16E-03
GO:0005618	cell wall	72	550	33.90	1.16E-03
GO:0010383	cell wall polysaccharide metabolic process	22	93	5.73	1.16E-03
GO:0030312	external encapsulating structure	72	552	34.03	1.16E-03
GO:0010143	cutin biosynthetic process	11	26	1.60	1.16E-03
GO:0009808	lignin metabolic process	14	42	2.59	1.16E-03
GO:0009832	plant-type cell wall biogenesis	30	153	9.43	1.16E-03
GO:0010410	hemicellulose metabolic process	18	68	4.19	1.23E-03
GO:0044038	cell wall macromolecule biosynthetic process	17	63	3.88	1.46E-03
GO:0070589	cellular component macromolecule biosynthetic process	17	63	3.88	1.46E-03
GO:0071554	cell wall organization or biogenesis	57	407	25.09	2.71E-03
GO:0071669	plant-type cell wall organization or biogenesis	42	267	16.46	2.90E-03
GO:0044036	cell wall macromolecule metabolic process	25	125	7.71	3.14E-03
GO:0009505	plant-type cell wall	42	276	17.01	3.46E-03
GO:0044550	secondary metabolite biosynthetic process	33	190	11.71	3.55E-03
GO:0045492	xylan biosynthetic process	13	43	2.65	3.70E-03
GO:0070592	cell wall polysaccharide biosynthetic process	16	62	3.82	3.86E-03
GO:0010025	wax biosynthetic process	11	31	1.91	5.67E-03
GO:0006649	phospholipid transfer to membrane	5	8	0.49	6.55E-03
GO:0010166	wax metabolic process	11	35	2.16	1.61E-02
GO:0019748	secondary metabolic process	39	266	16.40	1.95E-02
GO:1901570	fatty acid derivative biosynthetic process	11	37	2.28	3.02E-02
GO:1901957	regulation of cutin biosynthetic process	7	17	1.05	3.02E-02
GO:0016841	ammonia-lyase activity	6	12	0.74	4.20E-02
GO:0005576	extracellular region	53	440	27.12	4.76E-02
GO:0005875	microtubule associated complex	19	99	6.10	5.36E-02
GO:0000786	nucleosome	5	11	0.68	5.36E-02
GO:0045548	phenylalanine ammonia-lyase activity	4	5	0.31	6.54E-02
GO:0010090	trichome morphogenesis	16	78	4.81	6.54E-02
GO:1901568	fatty acid derivative metabolic process	13	55	3.39	6.54E-02
GO:0005874	microtubule	19	101	6.23	7.20E-02
GO:0010158	abaxial cell fate specification	5	9	0.55	7.56E-02

593

594

595 **Table 3. Top 20 genes based on the log2 fold change between grooved and non-grooved zones.**

GO ID	Term	Annotated gene count	gene count in the cluster	Expected count	q-value
GO:0009834	plant-type secondary cell wall biogenesis	24	67	4.13	4.61E-07
GO:0009699	phenylpropanoid biosynthetic process	26	90	5.55	1.18E-05
GO:0009698	phenylpropanoid metabolic process	27	101	6.23	2.88E-05
GO:0042335	cuticle development	15	37	2.28	5.85E-05
GO:0042546	cell wall biogenesis	37	191	11.77	2.19E-04
GO:0009809	lignin biosynthetic process	14	38	2.34	6.37E-04
GO:0048046	apoplast	42	261	16.09	8.98E-04
GO:0045491	xylan metabolic process	16	53	3.27	1.16E-03
GO:0005618	cell wall	72	550	33.90	1.16E-03
GO:0010383	cell wall polysaccharide metabolic process	22	93	5.73	1.16E-03
GO:0030312	external encapsulating structure	72	552	34.03	1.16E-03
GO:0010143	cutin biosynthetic process	11	26	1.60	1.16E-03
GO:0009808	lignin metabolic process	14	42	2.59	1.16E-03
GO:0009832	plant-type cell wall biogenesis	30	153	9.43	1.16E-03
GO:0010410	hemicellulose metabolic process	18	68	4.19	1.23E-03
GO:0044038	cell wall macromolecule biosynthetic process	17	63	3.88	1.46E-03
GO:0070589	cellular component macromolecule biosynthetic process	17	63	3.88	1.46E-03
GO:0071554	cell wall organization or biogenesis	57	407	25.09	2.71E-03
GO:0071669	plant-type cell wall organization or biogenesis	42	267	16.46	2.90E-03
GO:0044036	cell wall macromolecule metabolic process	25	125	7.71	3.14E-03
GO:0009505	plant-type cell wall	42	276	17.01	3.46E-03
GO:0044550	secondary metabolite biosynthetic process	33	190	11.71	3.55E-03
GO:0045492	xylan biosynthetic process	13	43	2.65	3.70E-03
GO:0070592	cell wall polysaccharide biosynthetic process	16	62	3.82	3.86E-03
GO:0010025	wax biosynthetic process	11	31	1.91	5.67E-03
GO:0006649	phospholipid transfer to membrane	5	8	0.49	6.55E-03
GO:0010166	wax metabolic process	11	35	2.16	1.61E-02
GO:0019748	secondary metabolic process	39	266	16.40	1.95E-02
GO:1901570	fatty acid derivative biosynthetic process	11	37	2.28	3.02E-02
GO:1901957	regulation of cutin biosynthetic process	7	17	1.05	3.02E-02
GO:0016841	ammonia-lyase activity	6	12	0.74	4.20E-02
GO:0005576	extracellular region	53	440	27.12	4.76E-02
GO:0005875	microtubule associated complex	19	99	6.10	5.36E-02
GO:0000786	nucleosome	5	11	0.68	5.36E-02
GO:0045548	phenylalanine ammonia-lyase activity	4	5	0.31	6.54E-02
GO:0010090	trichome morphogenesis	16	78	4.81	6.54E-02
GO:1901568	fatty acid derivative metabolic process	13	55	3.39	6.54E-02
GO:0005874	microtubule	19	101	6.23	7.20E-02
GO:0010158	abaxial cell fate specification	5	9	0.55	7.56E-02

596